New Photometric Observations and the First Wilson Program Analysis of the Totally Eclipsing, Solar Type Binary, UU Camelopardalis

Ronald G. Samec
Pisgah Astronomical Research Institute, 112 Idlewood Acres, Hartwell, GA 30643; ronaldsamec@gmail.com

Daniel Caton
Dark Sky Observatory, Department of Physics and Astronomy, Appalachian State University, 525 Rivers Street, Boone, NC 28608-2106; catondb@appstate.edu

Danny Faulkner
Johnson Observatory, 1414 Bur Oak Court, Hebron, KY 41048; dfaulkner@answersingenesis.org

Received July 1, 2022; revised August 5, 11, 2022; accepted August 12, 2022

Abstract CCD BVRI light curves of UU Cam were taken on 19, 20, 21, 23, 24, and 27 January 2021 by Daniel Caton at the Dark Sky Observatory, North Carolina, with the 0.81-m reflector of Appalachian State University. The variability of UU Cam was discovered by Baker. UU Cam is an eclipsing binary with a totally eclipsing secondary. The eclipse duration is some 54 minutes. The period behavior is quadratic following JD 2454860. Before this, there appears to be a constant period or the scatter is very high. There are 34 timings in the period study covering an interval of ~29.6 years. From our study, the period is found to be increasing. This could be due to mass transfer making the mass ratio decrease. A Wilson-Devinney analysis reveals that the system is an A-type (most massive component is the hottest) W UMa binary with a fairly extreme mass ratio, q = 0.2551 ± 0.0002. Its Roche Lobe fill-out is an extreme ~60%. One cool spot was needed in the solution. The temperature difference of the components is only ~121 K. The inclination is high, 82.04 ± 0.05, resulting in a time of constant light in the primary eclipse.

1. Introduction

The variability of UU Cam was discovered by Baker (1937). He gives a photographic magnitude range of 11.6–12.5. Bond (1978) identified UU Cam spectra as that those of an RR Lyrae variable. Poretti (1986) took the first B, V measures and confirmed substantially that the variable was an RR Lyrae. What we now have identified as the secondary minimum total eclipse was not covered in their light curve. It has been argued that the period changes probably showed long-term light time effects of another body orbiting UU Cam (Liska and Skarka 2015).

A number of IBVS articles contain minima from 2005 on and all refer to UU Cam as an eclipsing binary. This is probably due to the secondary total eclipse as seen in the ASAS-SN curves (Shappee *et al.* 2014; Kochanek *et al.* 2017) seen as Figure 1. This eclipsing binary system was observed by the All-Sky Automated Survey as ASASSN-V J051858.09+365806.2 (Pojmański 2002; Jayasinghe *et al.* 2019). They give a V_{mean} of 11.61, an amplitude of 0.49, an EW designation, and a J–K = 0.205. Their ephemeris is:

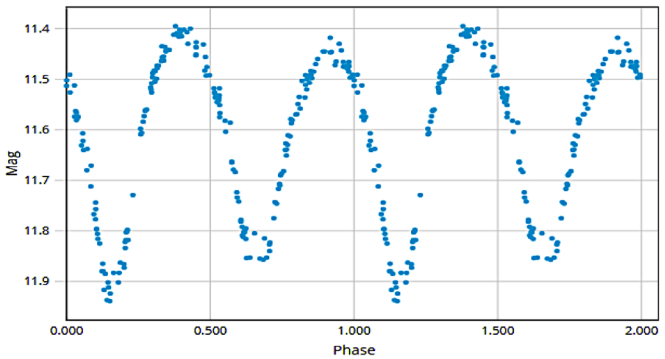

Figure 1. V-ASAS-SN light curves, ASASSN-V J035217.64+743356.8 (Shappee *et al.* 2014).

$$\text{HJD Min I} = 2457769.92503 + 0.6825577\,\text{d} \times \text{E} \quad (1)$$

From the ASAS-SN curves we were able to phase the data with Equation 1 and do parabola fits to the primary and secondary minima to locate seven times of "low light" within 0.001 phase of each minimum (these were weighted 0.1). We also included the ASAS-SN HJD Min I in our period study. This system was observed as a part of our professional collaborative studies of interacting binaries at Pisgah Astronomical Research Institute from data taken from DSO observations. The observations were taken by D. Caton, R. Samec, and D. Faulkner. Reduction and analyses were done by R. Samec.

A sample of the first ten sets of observations is given in Table 1. The complete table is available through the AAVSO ftp site as given in the table.

Our BVRI light curves were taken at Dark Sky Observatory, on 19–21, 23, 24, and 27 January 2021, with a thermoelectrically cooled (–35° C) 1KX1K FLI camera and Bessell filters.

Individual observations included 830 in B, 832 in V, 673 in R, and 666 in I. The probable error of a single observation was 4 mmag in B, V, and R, and 3 mmag in I. The nightly C–K values stayed constant throughout the observing run with a precision of about 1%. Exposure times varied from 45s in B, 20s in V, and 15s in R and I. To produce these images, nightly images were calibrated with 25 bias frames, at least five flat frames in each filter, and ten 300-second dark frames.

Table 1. Sample of first ten UU Cam *B, V, R, I* observations.

ΔB	*HJD 2459230+*	ΔV	*HJD 2459230+*	ΔR	*HJD 2459230+*	ΔI	*HJD 2459230+*
–0.1310	3.6189	–0.0450	3.6160	0.0160	3.6205	0.0650	3.6208
–0.0970	3.6243	–0.0310	3.6214	0.0170	3.6216	0.0770	3.6218
–0.1050	3.6254	–0.0250	3.6224	0.0300	3.6227	0.0750	3.6229
–0.0920	3.6264	–0.0230	3.6235	0.0190	3.6237	0.0780	3.6240
–0.0920	3.6275	–0.0220	3.6246	0.0400	3.6248	0.0800	3.6250
–0.0810	3.6286	–0.0190	3.6257	0.0290	3.6259	0.0930	3.6261
–0.0850	3.6297	–0.0160	3.6267	0.0380	3.6270	0.0820	3.6272
–0.0740	3.6308	–0.0150	3.6278	0.0510	3.6280	0.0950	3.6283
–0.0840	3.6318	0.0010	3.6300	0.0450	3.6291	0.0990	3.6294
–0.0710	3.6329	0.0070	3.6311	0.0470	3.6302	0.1070	3.6304

Note: First ten data points of UU Cam B, V, R, I observations. The complete table is available through the AAVSO ftp site at ftp://ftp.aavso.org/public/datasets/3844-Samec-502-uucam.txt (if necessary, copy and paste link into the address bar of a web browser).

Table 2. Photometric targets.

Role	*Label*	*Name*	*V*	*J–K (2MASS)*
Variable	V	UU Cam, GGM2006 6868894	11.45	0.205 ± 0.033, F5V
Comparison	C	GSC 4339 2245	11.79	0.326 ± 0.035, G0V
Check	K	GSC 4339 1108	13.58	0.32 ± 0.04, G0V

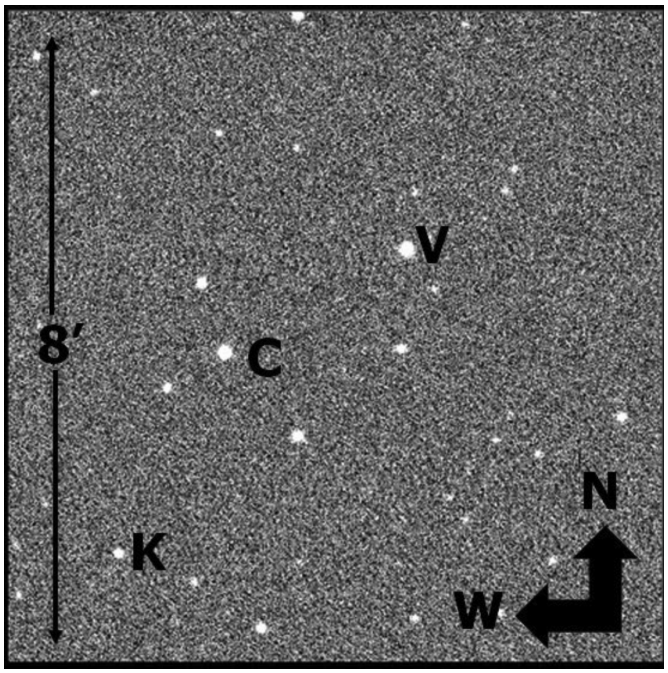

Figure 2. Finding chart of V, the variable star (UU Cam), C, the comparison star (GSC 4339 2245), and K, the check star (GSC 4339 1108).

2. Target stars

The finding chart of the observational field is shown in Figure 2. The target stars are given in Table 2.

3. Period determination

Four mean times (from BVRI data) of minimum light were calculated from our present observations, two primary and two secondary eclipses: the period behavior appears to be quadratic following JD 2448680.67 (Paschke 2020). Before this there appears to be a constant period or the scatter is very high. So, this study is from that of JD 2448680.67 and thereafter (Table 3). The minima mentioned above were weighted as 1.0 in this period study. The single filter minima of multicolor groups were weighted as 0.3. In addition, ten times minima were taken from *IBVS* and two from *BAVM*. Nine times were taken from *MVS*. Seven ASAS-SN times of minimum light were included in the study and weighted as 0.1. This gave us 34 timings in the period study with an interval of ~29.6 years.

From these timings, two ephemerides have been calculated, a linear and a quadratic one:

$$\text{JD Hel Min I} = 2459241.54719 \pm 0\ .00098\,\text{d} + 0.\ 68255861 \pm 0.00000016 \times \text{E} \quad (2)$$

$$\text{JD Hel Min I} = 2459241.55093 \pm 0.00072\text{d} + 0.\ 68256120 \pm 0.00000027\text{E} + 0.000000000212 \pm 0.000000000020 \times \text{E}^2 \quad (3)$$

Equation 3 shows an orbital period that is increasing, as shown in the O–C curve in Figure 3. This might be due to mass transfer to the more massive, primary component, making the mass ratio more extreme. However, this curve could be part of a longer period sinusoid.

The quadratic ephemeris yields a $\dot{\text{P}} = 2.27 \times 10^{-7}$ d/yr or a mass exchange rate of

$$\frac{\text{dM}}{\text{dt}} = \frac{\dot{\text{P}}\,\text{M}_1\,\text{M}_2}{3\text{P}\,(\text{M}_1 - \text{M}_2)} = \frac{5.58 \times 10^{-8}\,\text{M}_\odot}{\text{yr}}. \quad (4)$$

in a conservative scenario (the primary component is the gainer).

Table 3. UU Cam O–C.

Minima 2400000+	*Cycles*	*Linear Residuals*	*Quadratic Residuals*	*Weight*	*Reference*
48680.6700	–15472.5	0.0109	–0.0033	1.0	Schmidt *et al.* (1995)
51349.1290	–11563.0	0.0070	0.0050	1.0	Paschke (2020)
52685.5697	–9605.0	–0.0020	–0.0003	1.0	Hubscher *et al.* (2005)
53450.0349	–8485.0	–0.0025	0.0006	1.0	Kim *et al.* (2006)
54811.7390	–6490.0	–0.0028	0.0014	1.0	Diethelm (2009)
55121.9640	–6035.5	–0.0007	0.0035	1.0	Diethelm (2010)
55125.3768	–6030.5	–0.0007	0.0035	1.0	Hübscher *et al.* (2010)
55566.6466	–5384.0	–0.0050	–0.0009	1.0	Diethelm (2011)
55670.3962	–5232.0	–0.0043	–0.0003	1.0	Hübscher *et al.* (2012)
55849.9057	–4969.0	–0.0078	–0.0038	1.0	Diethelm (2012)
55942.3979	–4833.5	–0.0022	0.0016	1.0	Hübscher and Lehmann (2012)
55969.3566	–4794.0	–0.0046	–0.0008	1.0	Hübscher and Lehmann (2012)
56297.6653	–4313.0	–0.0066	–0.0031	1.0	Diethelm (2013)
57374.7333	–2589.0	–0.0056	–0.0041	0.1	Shappee *et al.* (2014); Kochanek *et al.* (2017)
58322.1247	–2735.0	–0.0161	–0.0143	0.1	Shappee *et al.* (2014); Kochanek *et al.* (2017)
57320.1328	–1347.0	–0.0160	–0.0166	0.1	Shappee *et al.* (2014); Kochanek *et al.* (2017)
58128.9647	–2815.0	–0.0119	–0.0100	0.1	Shappee *et al.* (2014); Kochanek *et al.* (2017)
58018.0506	–1630.0	–0.0120	–0.0120	0.1	Shappee *et al.* (2014); Kochanek *et al.* (2017)
57020.8467	–1792.5	–0.0103	–0.0101	0.1	Shappee *et al.* (2014); Kochanek *et al.* (2017)
57046.7917	–3253.5	0.0039	0.0064	0.1	Shappee *et al.* (2014); Kochanek *et al.* (2017)
57474.3973	–3215.5	0.0117	0.0141	1.0	Hübscher (2017)
57844.3444	–2047.0	–0.0053	–0.0046	1.0	Lehký *et al.* (2021)
58771.2650	–689.0	0.0007	–0.0014	1.0	Pagel (2020)
59061.3499	–264.0	–0.0018	–0.0049	0.3	Auer 2021
59061.3520	–264.0	0.0003	–0.0028	0.3	Auer 2021
59061.3550	–264.0	0.0033	0.0002	0.3	Auer 2021
59062.3801	–262.5	0.0045	0.0015	0.3	Auer 2021
59062.3821	–262.5	0.0065	0.0035	0.3	Auer 2021
59062.3824	–262.5	0.0068	0.0038	0.3	Auer 2021
59233.7062	–11.5	0.0085	0.0048	1.0	Present Observations
59234.7265	–10.0	0.0049	0.0012	1.0	Present Observations
59237.8007	–5.5	0.0076	0.0039	1.0	Present Observations
59241.5511	0.0	0.0039	0.0002	1.0	Present Observations
59489.3212	363.0	0.0052	0.0005	1.0	Pagel (2022)

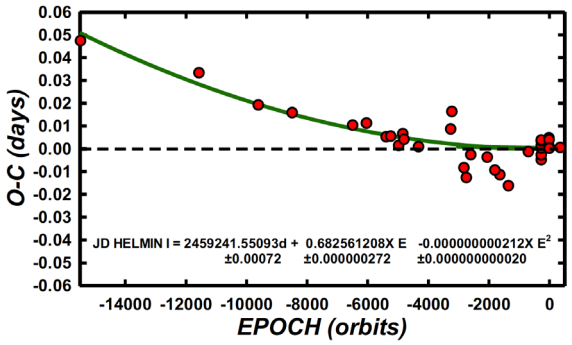

Figure 3. Quadratic O–C residuals.

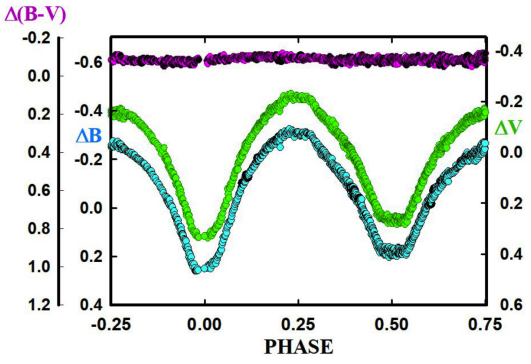

Figure 4. B, V, and B–V magnitude phased plots with the new linear ephemeris, Equation 2.

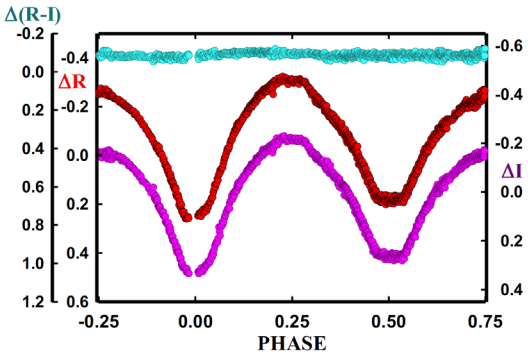

Figure 5. R, I, and R–I magnitude phased plots with the new linear ephemeris, Equation 2.

4. Light curve characteristics

The B, V, B–V, and R, I, and R–I mags were phased with the new linear ephemeris, Equation 2. These phased plots are given in Figures 4 and 5.

The quarter-cycle light curve characteristics of B, V, R, and I plots are given in Table 4.

The curves are of good accuracy, averaging about 2% photometric precision. The noise is probably due to magnetic activity. The amplitude of the light curve varies from 0.507 to 0.551 for I to B magnitudes. The O'Connell effect, an indicator

Table 4. Light curve characteristics.

Filter	*Phase Min I*	*Error*	*Phase Max I*	*Error*		
	0.00	± σ	0.25	± σ		
B	0.243	0.006	–0.308	0.009		
V	0.332	0.004	–0.216	0.008		
R	0.383	0.007	–0.151	0.007		
I	0.420	0.003	–0.087	0.007		
	Min II		Max II			
	0.50	± σ	0.75	± σ		
B	0.183	0.012	–0.257	0.009		
V	0.265	0.009	–0.154	0.008		
R	0.317	0.006	–0.108	0.007		
I	0.372	0.007	–0.058	0.007		
	Min I – Max I	± σ	Max II – Max I	± σ	Min I – Min II	± σ
B	0.551	0.014	0.051	0.017	0.060	0.018
V	0.547	0.012	0.062	0.015	0.066	0.013
R	0.534	0.014	0.043	0.013	0.066	0.014
I	0.507	0.010	0.029	0.013	0.048	0.010
	Min II– Max I	± σ	Min I – Max II	± σ	Min II– Max II	± σ
B	0.491	0.021	0.500	0.014	0.440	0.021
V	0.481	0.016	0.485	0.012	0.419	0.016
R	0.468	0.013	0.491	0.014	0.425	0.013
I	0.459	0.013	0.478	0.010	0.429	0.013

Table 5. B,V,R,I Solution parameters.

Parameters	*Values*
$\lambda_B, \lambda_V, \lambda_R, \lambda_I$ (nm)	440, 550, 640, 790
g_1, g_2	0.32
A_1, A_2	0.50
Inclination (°)	82.040 ± 0.050
T_1, T_2 (K)	6500, 6379 ± 1
$\Omega_1 = \Omega_2$	2.268 ± 0.001
$q(m_1/m_2)$	0.255 ± 0.000
Fill-outs: F(%)	60.1(0.5)
$L_1/(L_1+L_2)_I$	0.771 ± 0.002
$L_1/(L_1+L_2)_R$	0.773 ± 0.002
$L_1/(L_1+L_2)_V$	0.775 ± 0.003
$L_1/(L_1+L_2)_B$	0.779 ± 0.003
JD_o (days)	2459241.5516 ± 0.0001
Period (days)	0.68257 ± 0.00001
Dimensions:	
$r_1/a, r_2/a$ (pole)	0.490 ± 0.001, 0.274 ± 0.001
$r_1/a, r_2/a$ (side)	0.537 ± 0.001, 0.289 ± 0.001
$r_1/a, r_2/a$ (back)	0.616 ± 0.001, 0.351 ± 0.003
Spot, primary component	Cool spot region
Colatitude (°)	71.8 ± 0.5
Longitude (°)	105.6 ± 0.3
Radius (°)	24.71 ± 0.07
T-Factor	0.919 ± 0.0011

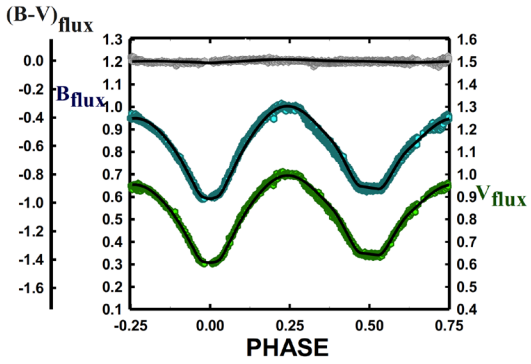

Figure 6. B, V, and B–V normalized fluxes overlaid by the light curve solution.

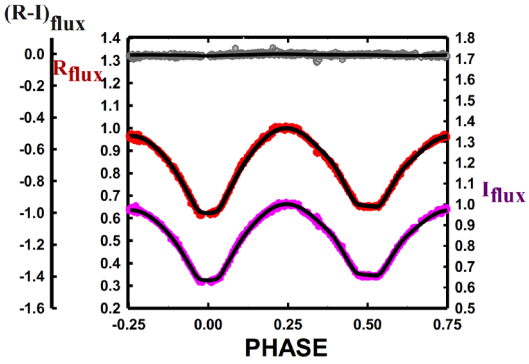

Figure 7. R, I, and R–I normalized fluxes overlaid by the light curve solution.

Table 6. UU Cam system dimensions.

R_1, R_2 (pole, $R_\odot$)	1.89 ± 0.002	0.669 ± 0.0003
R_1, R_2 (side, $R_\odot$)	2.07 ± 0.003	0.700 ± 0.0003
R_1, R_2 (back, $R_\odot$)	2.20 ± 0.003	0.844 ± 0.0004

Table 7. Estimated absolute parameters1.

Parameter	*Star 1*	*Star2*
Mean radius ($R_\odot$)	2.053 ± 0.009	0.738 ± 0.004
Mean density	0.212 ± 0.004	0.303 ± 0.006
Mass ($M_\odot$)	1.35 ± 0.01	0.37 ± 0.01
Log g	3.94	3.86

Note: Using light curve solution units, a = 1, a is calculated for Wilson program, the semi-major axis. Density is in g/cm³, a = 3.8568 $R_\odot$ (Bradstreet and Steelman 2002).

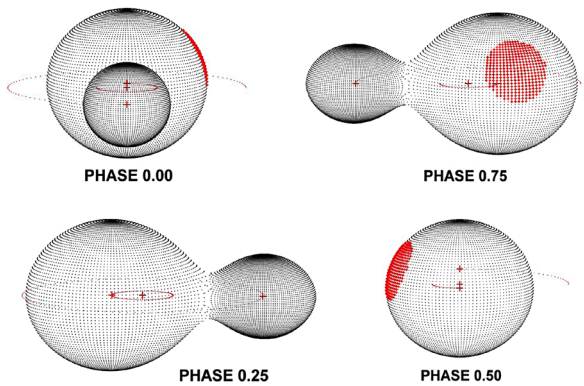

Figure 8. UU CAM, geometrical representation at quarter orbital phases.

of spot activity, was 0.051 to 0.029 magnitude, B to I, indicating magnetic activity. The difference in minima, 0.060 to 0.048 for B to I, indicates over contact light curves that could be in good thermal contact. A time of constant light occurs at our secondary minima and lasts some 54 minutes.

5. Light curve solution

The 2MASS, J–K = 0.205 ± 0.033 for the binary star; this corresponds to ~F5V ± 2.5, which yields a temperature of 6500 ± 200 K. Fast rotating binary stars of this type are noted for having strong magnetic activity, so the binary is of solar type with a convective atmosphere. The B, V, R, and I curves were pre-modeled with Binary Maker 3.0 (Bradstreet and Steelman 2002). Fits were determined in all filter bands which were very stable. The solution was that of an over contact eclipsing binary. The parameters were then averaged (q = 0.24, fill-out = 0.7, i = 81.5°, T_2 = 6394 K, with one 17° cool spot, T-FACT = 0.785) and input into a four-color simultaneous light curve calculation using the Wilson-Devinney Program (Wilson and Devinney 1971; Wilson 1990, 1994, 2004; van Hamme and Wilson 1998). The solution (Table 4) was computed in Mode 3 and converged to a solution. Convective parameters, g = 0.32, A = 0.5 were used. An eclipse duration of ~54 minutes was determined for our secondary eclipse and the light curve solution. Due to the total eclipses, the mass ratio, q, is well determined. The more massive component is the hottest one, making the system a A-type W UMa over contact binary. Third light was tried but ended with negative brightness values. The solution follows as Table 5. The normalized fluxes overlaid by our solution of UU Cam in B,V,R,I are shown in Figures 6 and 7, and the Roche Lobe representation at quarter orbital phases is shown in Figure 8. System dimensions (Tables 6 and 7) were calculated from the value of the semimajor axis, required by the Wilson program determined from Kepler's Law (with the mass ratio, period, and the estimated primary mass from the primary temperature), the stellar densities are found exactly from the orbital period and Binary Maker (contact mode from Roche Lobe equations), and radius values from the Wilson program. The volumes (from the average radius) and the densities give the mass of the two components. The log g values follow from GM/r^2.

6. Discussion

UU Cam is a A-type, W UMa binary. Since the eclipses were total, the mass ratio, q = 0.255, is well determined with a fill-out of 60%. The system has a component temperature difference of ~121 K, so it is in good thermal contact. One spot was needed in the final modeling. The inclination of ~82 degrees resulted in a ~50-minute time of constant light in the secondary eclipse. Its photometric spectral type indicates a surface temperature of ~6500 K for the primary component, making it a solar type binary. The calculated masses (see Table 7) are very near the main sequence star mass of ~1.33 $M_\odot$ (F5V) and the secondary (from the mass ratio) mass of ~0.34 $M_\odot$, making it very much undersized. The temperature of the secondary component (~6379 K) of a main sequence star would make it of type F6V instead of M3V as indicated by its mass.

7. Conclusion

The period of this binary indicates that it is increasing. This could be due to mass exchange with the flow toward the more massive component,

$$\frac{dM}{dt} = \frac{5.58 \times 10^{-8}\, M_\odot}{yr}, \qquad (5)$$

making the mass ratio more extreme (M_1/M_2 smaller). The mass ratio is approaching that of an extreme mass ratio binary as noted in many other of the authors' papers (Caton *et al.* 2019; Samec *et al.* 2017, 2015, 2012, and earlier). This means the two components may coalesce in time, making it, presently, a red novae progenitor. Combined with the high fill-out, this system is approaching the characteristics of Deep Low-Mass Ratio (DLMR) systems (Qian *et al.* 2005).

8. Future work

Radial velocity curves are needed to obtain absolute (not relative) system parameters.

References

Auer, R. F. 2021, *Open Eur. J. Var. Stars*, **210**, 1.
Baker, E. A. 1937, *Mon. Not. Roy. Astron. Soc.*, **98**, 65.
Bond, H. E. 1978, *Publ. Astron. Soc. Pacific*, **90**, 526.
Bradstreet, D. H., and Steelman, D. P. 2002, *Bull. Amer. Astron. Soc.*, **34**, 1224.
Caton, D., Gentry, D. R., Samec, R. G., Chamberlain, H., Robb, R., Faulkner, D. R., and Hill, R. 2019, *Publ. Astron. Soc. Pacific*, **131**, 054203.
Diethelm, R. 2009, *Inf. Bull. Var. Stars*, No. 5871, 1.
Diethelm, R. 2010, *Inf. Bull. Var. Stars*, No. 5920, 1.
Diethelm, R. 2011, *Inf. Bull. Var. Stars*, No. 5992, 1.
Diethelm, R. 2012, *Inf. Bull. Var. Stars*, No. 6011, 1.
Diethelm, R. 2013, *Inf. Bull. Var. Stars*, No. 6063, 1.
Hübscher, J. 2017, *Inf. Bull. Var. Stars*, No. 6196, 1.
Hübscher, J. and Lehmann, P. B. 2012, *Inf. Bull. Var. Stars*, No. 6026, 1.
Hübscher, J. Lehmann, P. B., Monninger, G., Steinbach, H. M., and Walter, F. 2010, *Inf. Bull. Var. Stars*, No. 5941, 1.
Hübscher, J. Lehmann, P. B., and Walter, F. 2012, *Inf. Bull. Var. Stars*, No. 6010, 1.
Hübscher, J. Paschke, A., and Walter, F. 2005, *Inf. Bull. Var. Stars*, No. 5657, 1.
Jayasinghe, T., *et al.* 2019, *Mon. Not. Roy. Astron. Soc.*, **486**, 1907.
Kim, C.-H., Lee, C.-U., Yoon, Y.-N., Park, S.-S., Kim, D.-H., Cha, S.-M., and Won, J.-H. 2006, *Inf. Bull. Var. Stars*, No. 5694, 1.
Kochanek, C. S., *et al.* 2017, *Publ. Astron. Soc. Pacific*, **129**, 104502.
Lehký, M., *et al.* 2021, *Open Eur. J. Var. Stars*, **211**, 1.
Liška,, J., and Skarka, M. 2015, *Open Eur. J. Var. Stars*, **169**, 38.
Pagel, L. 2020, *BAV J.*, No. 33, 1.
Pagel, L. 2022, *BAV J.*, No. 60, 1.
Paschke, A. 2020, O–C Gateway (http://var.astro.cz/ocgate/).

Pojmański, G. 2002, *Acta Astron.*, **52**, 397.
Poretti E. 1986, *Astrophys. Space Sci.*, **126**, 329.
Qian, S.-B., Yang, Y.-G., Soonthornthum, B., Zhu, L.-Y., He, J.-J., and Yuan, J.-Z. 2005, *Astron. J.*, **130**, 224.
Samec, R. G., Benkendorf, B., Dignan, J. B., Robb, R., Kring, J., and Faulkner, D. R. 2015, *Astron. J.*, **149**,146.
Samec, R. G., Figg, E. R., Labadorf, C. M., Faulkner, D. R., and van Hamme, W. 2012, *Observatory*, **132**, 98.
Samec, R. G., Gray, C. R., Caton, D., Faulkner, D. R., Hill, R., and van Hamme, W. 2017, *J. Amer. Assoc. Var. Star Obs.*, **45**, 140.
Schmidt, E. G., Chab, J. R, and Reiswig, D. E. 1995, *Astron. J.*, **109**, 1239.
Shappee, B. J., *et al.* 2014, *Astrophys. J.*, **788**, 48.
van Hamme, W. V., and Wilson, R. E. 1998, *Bull. Amer. Astron. Soc.*, **30**, 1402.
Wilson, R. E. 1990, *Astroophys. J.*, **356**, 613.
Wilson, R. E. 1994, *Publ. Astron. Soc. Pacific*, **106**, 921.
Wilson, R. E. 2004, *New Astron. Rev.*, **48**, 695.
Wilson, R. E., and Devinney, E. J. 1971, *Astrophys. J.*, **166**, 605.